Dynamics of swimming bacteria: Transition to directional order at high concentration

Luis H. Cisneros, John O. Kessler, Sujoy Ganguly, and Raymond E. Goldstein

Phys. Rev. E **83**, 061907 — Published 14 June 2011

DOI: 10.1103/PhysRevE.83.061907

Dynamics of swimming bacteria: transition to directional order at high concentration

Luis H. Cisneros* and John O. Kessler†
University of Arizona Department of Physics, 1118 E. 4th St., Tucson, AZ 85721

Sujoy Ganguly‡ and Raymond E. Goldstein§
Department of Applied Mathematics and Theoretical Physics, Centre for Mathematical Sciences, University of Cambridge, Wilberforce Road, Cambridge CB3 0WA, UK

At high cell concentrations bacterial suspensions are known to develop a state of collective swimming (the 'Zooming BioNematic Phase' or ZBN) characterized by transient, recurring regions of coordinated motion greatly exceeding the size of individual cells. Recent theoretical studies of semi-dilute suspensions have suggested that long-range hydrodynamic interactions between swimming cells are responsible for long-wavelength instabilities that lead to these patterns, while models appropriate to higher concentrations have suggested that steric interactions between elongated cells play an important role in the self-organization. Using particle imaging velocimetry in well-defined micro-geometries, we examine the statistical properties of the transition to the ZBN in suspensions of *Bacillus subtilis*, with particular emphasis on the distribution of cell swimming speeds and its correlation with orientational order. This analysis reveals a non-monotonic relationship between mean cell swimming speed and cell concentration, with a minimum occurring near the transition to the ZBN. Regions of high orientational order in the ZBN phase have locally high swimming speeds, while orientationally disordered regions have lower speeds. A model for steric interactions in concentrated suspensions and previous observations on the kinetics of flagellar rebundling associated with changes in swimming direction are used to explain this observation. The necessity of incorporating steric effects on cell swimming in theoretical models is emphasized.

PACS numbers: 87.18.Gh,05.65.+b,47.20.-k, 47.54.-r

I. INTRODUCTION

It is now well-established that a concentrated population of bacterial cells may develop into a 'super-organism' with properties and capabilities that extend beyond those of single individuals [1, 2]. On the one hand, the organized internal dynamics of such 'multicellular' organisms arises from the coordination of the physics of propulsion and the shape of its members rather than direct cellular communication, yet it has direct effects on biological processes associated with chemical signaling. Collectively stimulated emission and sensing of chemical messengers by members of a bacterial culture can lead to formation of biofilms [3]. On the other hand, a distinct phenomenon, swarming, comprises changes in the morphology of individual members of the population associated with increased motility and collective directionality [4–6].

Concentrated swimming organisms induce strong local flows in the embedding fluid medium, affecting the motion of neighboring cells and ultimately producing large-scale instabilities that develop into complex chaotic dynamics characterized by fast and locally aligned cells [7–11]. For sufficiently high concentrations of rod-shaped bacteria, coherence is observed in the form of collective motion, often faster than the motion of individual swimming cells, and in a narrow angular distribution of velocities within spontaneously appearing domains. A movie of this state (see Supplemental Material [12]) shows local parallel alignment of cells that is reminiscent of nematic liquid crystals, and these domains aggregate, rush and twist, break up and re-form in a manner reminiscent of turbulence, giving the impression of zooming about: thus the acronym ZBN, for 'Zooming BioNematic." The intermittency of the ZBN greatly enhances the transport of dissolved molecules or suspended particles, beyond normal diffusion. In this way, intercellular signaling, acquisition of metabolites, elimination of molecular wastes, and dispersal of extracellular products are greatly enhanced by the dynamics of the highly concentrated coherent state.

Theoretical approaches to collective motion of self-propelled particles began with highly simplified models of flocking using ideas from statistical physics [13–15]. These led to the notion of a nonequilibrium phase transition to a state

*Electronic address: cisneros@physics.arizona.edu
†Electronic address: kessler@physics.arizona.edu
‡Electronic address: S.Ganguly@damtp.cam.ac.uk
§Electronic address: R.E.Goldstein@damtp.cam.ac.uk

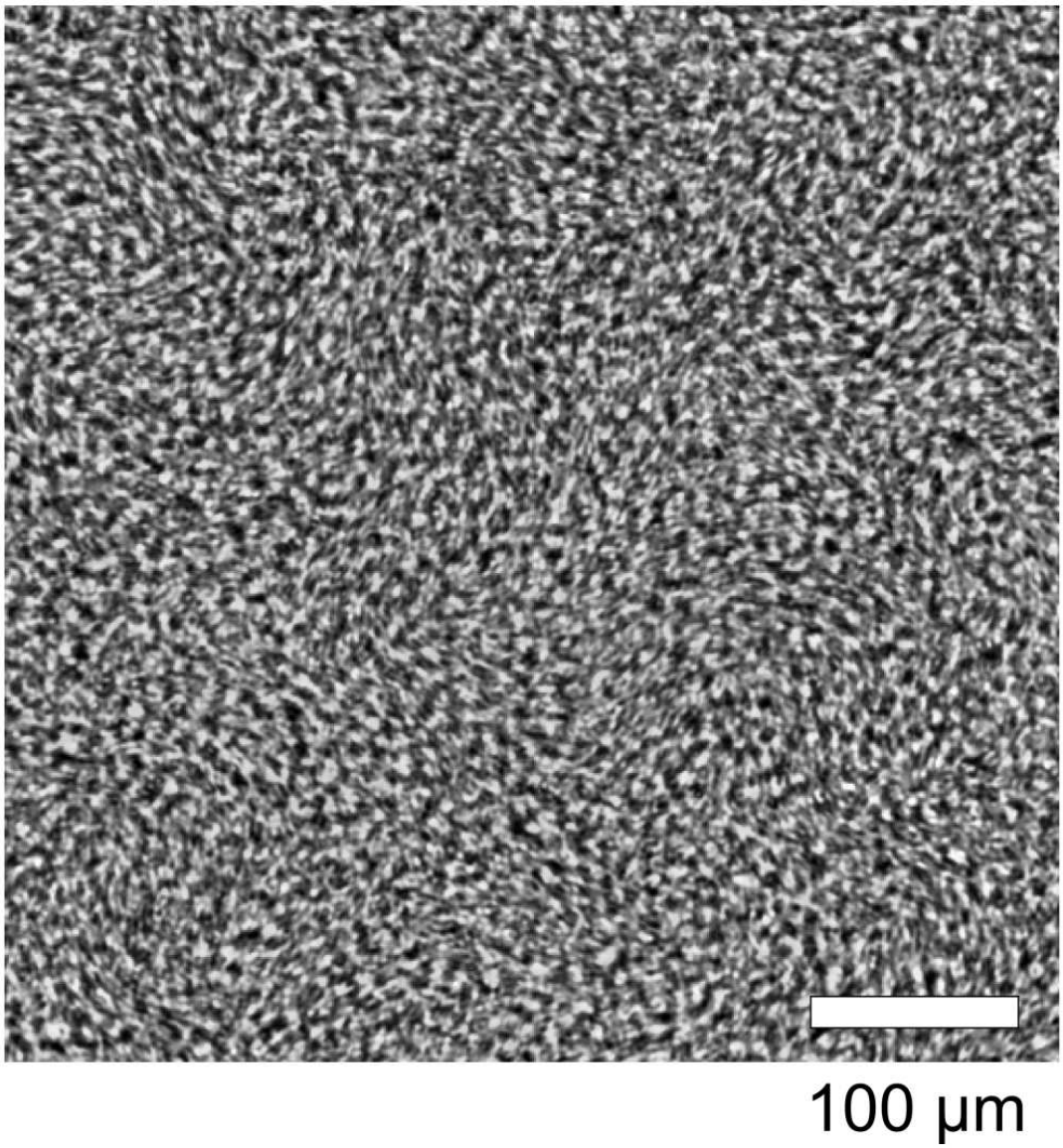

FIG. 1: Image of a suspension of swimming *B. subtilis* in the ZBN phase. Bacterial cells occupy both bright and dark spots in the image. The difference between bright and dark is due to orientation of the cylindrical cell bodies relative to the optic axis and displacement from the focal plane. See also movie 3 of Supplemental Material [12]).

with *long-range* order in the swimming direction. Subsequent work [16] more faithful to the hydrodynamic interactions between swimming cells found a long-wavelength instability of that putative ordered state, and it has been suggested that this instability underlies the particular form of coherent structures found in the ZBN [10, 11]. Direct numerical simulations of two-sphere swimmers [17], one representing the cell body, the other the flagella, and rod-like swimmers with forces continuously distributed over their surfaces [18], and a comprehensive kinetic theory of these systems [19–21] has not only confirmed this finding but also begun to address the nature of the state beyond the instability. Other closely related models and approaches yield similar results [22]. Simulations [17, 23] found that passive tracers and swimmers exhibit super-diffusive behavior at short times and diffusive dynamics at long times, with the crossover depending on the concentration of swimmers. A two-phase model [24] exhibits the chaotic character of the collective bacterial swimming. These approaches provide the most likely current explanation for the transient, recurring vortices and jets observed in experiments to date on *B. subtilis* [10, 11], enhanced and anomalous diffusion of molecular species and tracer particles [7–9, 25], and a framework for addressing anomalous fluctuation statistics observed in more dilute solutions of swimming protists [26, 27].

The common ingredient in the kinetic theories cited above is a contribution to the stress tensor due to the self-propulsion of the organisms, represented by force dipoles (stresslets) [28]. It is clear from even casual observation of the ZBN, or indeed of less concentrated bulk suspensions (Fig. 1) or those in thin films [29] or on the surface of agar [30], that steric interactions between swimming cells must play an important role in establishing the local order, much as it does in liquid crystals and in models of "self-propelled rods" [15]. Theory [29] on collective dynamics of bacteria in suspended films [31] that incorporates not only hydrodynamic reorientation of cells in response to local fluid flows but also collisional realignment predicts an instability in the stress field at long wavelengths in the isotropic field.

In spite of these important contributions, there is a consistent lack of actual experimental results which can serve to inform further development of our understanding of the transition to collective behavior. In the present paper we provide new experimental results and a new set of theoretical considerations relevant to the appearance of the ZBN. Just as lyotropic liquid crystals exhibit order as a consequence of increasing concentration, the ZBN is a phase of suspended bacterial matter that emerges at high concentrations. At low concentrations, the swimming bacteria move essentially independently, but with increasing concentration we observe that an anomalous intermediate phase develops in which cellular collisions, characterized by stopping and then reconstitution of the propulsion mechanism, produce a slowing of the mean swimming speeds relative to those observed for free individual cells. We shall term this the "jammed phase" (see Fig. 1) by analogy with concentrated automobile or pedestrian traffic. This contribution of flagellar interaction and bundling dynamics, which is absent in current models of bacterial collective dynamics, is suggested to be of significance when cells are in close proximity to each other.

The experimental observations and analyses reported here concern wild-type *Bacillus subtilis*, a rod-shaped gram positive bacterium. This paper thus considers collective behavior cells with no known mutations in the flagellar apparatus or motility. Our results delineate the sequence of steps leading from individual behaviors of normally motile *Bacillus subtilis* at low concentration to coherent, collective, sterically and hydrodynamically coupled dynamics at high concentration: a transition from individual to jammed state, to the collective ZBN state which depends strongly on sterically determined ordering, but whose ultimate dynamics depends on collectively synchronized motility and hydrodynamics.

The cells used here have a variable body length L, typically around 4μm, and a diameter $D \sim 1\mu$m. They are peritrichously flagellated, with a typical swimming speed $U \sim 25$ μm/s (see Fig. 3 below). The Reynolds number for such a swimming bacterium in water (kinematic viscosity $\nu = 0.01$ cm^2/s) is $\mathrm{Re} = UL/\nu \sim 10^{-4}$. The low value of Re indicates that viscous forces dominate over inertia and that the hydrodynamics is safely in the Stokes regime [32–34], thereby implying that the fluid flow generated by a swimming bacterium is completely driven by drag on the cell and its rotating flagella. (Here we neglect gravitational effects as our experiments involve thin samples in plan view). Previous experimental work has focused on using bacterial chemotaxis, the swimming of bacteria along chemical gradients, and self-concentration mechanisms [35], to concentrate cells near contact lines [10, 11] or in quasi two dimensional geometries [25, 31]. The typical observed collective speeds in the ZBN phase can be 100 μm/s, with an associated Reynolds number still $\ll 1$ (0.01 cm x 0.01 cm/s / 0.01 cm^2/s).

We present experiments on the dynamics away from solid boundaries and contact lines, uncovering some striking statistical signatures of the collective phase and the route to its emergence. In order to image the bacterial dynamics we perform video-microscopy with a high speed camera at 100 frames/second. This high frame rate allows us to record rapid changes in the microscopic system. Images are analyzed using Particle Image Velocimetry (PIV), a widespread technique employed in experimental fluid mechanics. Instantaneous velocity fields of the bacterial suspension are estimated directly from consecutive images, using a pattern matching procedure. This method yields statistical analyses and measures. Most notably, the distribution functions of cell velocities in the collective mode are found to differ radically from that of an equilibrium system, while for free swimming cells the speed distribution is approximately Maxwellian.

II. MATERIALS AND METHODS

All experiments were conducted with *Bacillus subtilis* strain 1085B. Stocks of cells were prepared by adding spores on sand to 10 ml of sterile Terrific Broth [TB: 48.2 g Ezmix Terrific Broth (Sigma) + 8 ml glycerol in sufficient water to make 1 l] at room temperature, and allowing the cells to grow and divide for 18 h. Then, 0.5 ml of this culture was mixed in equal parts with glycerol, frozen and stored at -20°C. The experimental samples were prepared by adding 1 ml of the -20°C stock to 10 ml of TB, allowing the culture to stand for 18 h in a petri dish, after which 1 ml of the bacterial suspension was added to 50ml of TB and incubated in a shaker bath (VWR model 1217; 37°C, 100 rpm) for 4 hours.

In order to concentrate the cells 1 ml of the 4-hour culture was placed in a vial (Eppendorf 1.6 ml) and centrifuged for 2 minutes at $4000g$, creating a loose pellet of bacteria. The supernatant was then removed and the bacteria-rich residue was re-suspended in the remaining medium. By controlling the amount of fluid used to re-suspend the cells

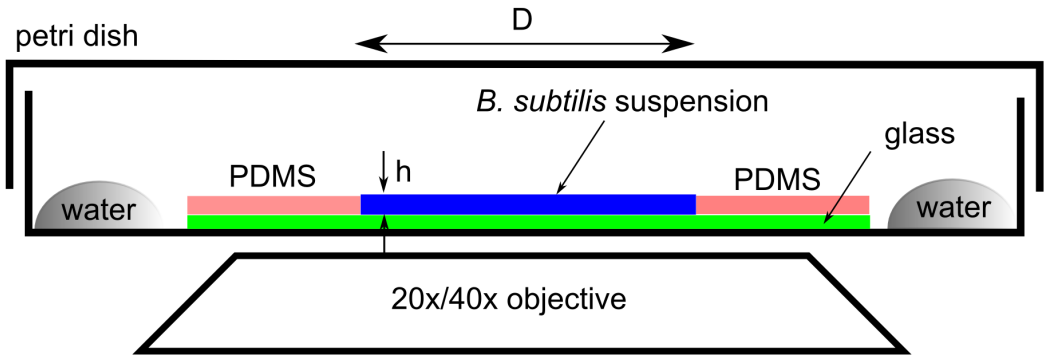

FIG. 2: (Color) Schematic of the experimental setup (not to scale); The bacterial suspension is deposited in a square well of sides $D = 5$ mm and depth $h = 100$ μm built over a glass slide with PDMS walls. This micro-chamber is placed in a closed petri dish with large water drops to control the evaporation of the sample, and imaged with a 20× or 40× objective on an inverted microscope.

we achieved coarse control of the final concentration. During each experiment, 5 μl of the concentrated sample was put in a solution of 10 μl iodine in 400 μl of 1 M NaCl to kill the bacteria. Samples of dead cells were diluted by a factor of 10 in 1 M NaCl and the bacteria were counted in a Neubauer Hemocytometer (Spencer Bright-Line 1490, American Optical Co.) for precise measurements of the cell concentration.

The microchambers used for experiments were square wells, 5 mm on a side and 0.1mm deep, constructed from polydimethylsiloxane (PDMS, Sylgard 184, Dow-Corning), using a hard plastic negative machined to high precision. The PDMS was degassed before being spread over the surface of the negative. Then, a clean glass slide, previously treated with Alconox in a sonicator for 10 minutes, was placed on top and weighed down to ensure uniform covering. Finally, the PDMS was cured in a vacuum oven for 18 h at 70°C. For each experiment, the chamber was filled with 5 μl of cell suspension and enclosed in a plastic petri dish with water reservoirs that provide a saturated environment to avoid sample evaporation (Fig. 2). The chambers were chosen to be shallow enough to inhibit the formation of bioconvection patterns [28, 36–39]. While small concentration gradients may still be expected for this geometry [39], they may be ignored at the level of detail presented in this paper.

Samples were imaged from below with an inverted microscope (Nikon Diaphot 300), using either a Nikon 40x PL APO (0.55NA) or a Nikon 20x PL APO (0.5NA) objective. The depth of field δz of each is [40]

$$\delta z = \frac{n_r \lambda_\ell}{\mathrm{NA}^2} + \frac{n_r e}{\mathrm{M(NA)}} \tag{1}$$

where $n_r \sim 1$ is the index of refraction of the air between the sample and the objective, $e = 16$ μm is the smallest distance that can be resolved by the detector (a pixel), λ_ℓ is the wavelength of light used to image, M is the magnification of the lens and NA is the its numerical aperture. When bright field illumination is used, the depth of field will be determined by the longest wavelength, $\lambda_\ell \sim 750$ nm. These give respective depths of field of $\delta z_{40\mathrm{x}} \sim 3.21$ μm and $\delta z_{20\mathrm{x}} \sim 4.8$ μm. Recalling the size of the bacterial cell body, we see that the depth of field resolves at most a couple of layers of cells.

Videos were obtained with a high speed camera (Phantom V5.1, Vision Research, Wayne, NJ) at 100 frames per second with a resolution of 1024×1024 pixels, which corresponds to fields of view of 813×813 μm^2 for the 20× objective and 403×403 μm^2 for the 40×. Sets of 500 frames were obtained for each experiment. Videos were processed to remove the background and increase the contrast. For the concentrations used there is significant overlapping of cells in the images (Fig. 1), so it is not possible to resolve individual bacteria. A commercial PIV system (Flow Manager, Dantec Dynamics) was used to estimate cell velocities. Most current digital PIV applications utilize a cross correlation analysis [41–43], in which each digital image is divided into small interrogation windows containing several tracers. Each of those interrogation windows is matched to a position in the successive image, which corresponds to the most likely displacement of the group of particles contained within it. All analyses presented here used an interrogation window 8×8 pixels (corresponding to regions 3.15 μm × 3.15 μm for the 40× magnification case, and 6.35 μm × 6.35 μm for 20×) with a 25% overlap. A uniform 3×3 averaging kernel was used to reduce the noise of the resulting field. The high accuracy needed for the experiments required correction for systematic errors in the PIV analysis, as detailed in the Appendix.

Particle tracking velocimetry (PTV) of individual bacterial trajectories in dilute conditions was used to describe the free swimming phase. These samples were prepared from the 4 h old culture as described above. One ml was

placed in a centrifuge chamber and spun down at $4000 \times g$ for 2 minutes and then resuspended and diluted to 1/100th of the original concentration. Samples were then put in a micro chamber and imaged. Thereafter, multiple cell trajectories are measured from the digital videos using a PTV program in MATLAB based original source code by Nicholas Darnton and Jacob D. Jaffe [44] with modifications by one of the authors (LHC) [45].

III. RESULTS AND DISCUSSION

The ZBN mode is a collective phase easy to identify when observed. Motion of adjacent cells is coherent in patches and appears as domains of fast motion that stretch, fold disperse and reconstitute, with incoherent regions between them. How may one characterize this phase in a quantitative manner useful for the validation of a model? An obvious place to start is by analyzing the probability distribution function (PDF) of speeds. In order to quantify the motion of uncrowded bacteria, individual trajectories were obtained from PTV on a dilute suspension (see movie 1 of Supplemental material [12]). A PDF based on the trajectories of the entire sample is shown in black in Fig. 3(a). Error bars indicate the standard errors associated with the average over trajectories. It is evident that the typical swimming speed of free cells falls in the range $15 - 30$ μm/s. This result agrees with previous data that also indicates higher speeds for a small component of the cell population [8, 46].

A PDF obtained in the ZBN phase using PIV is shown in red in Fig. 3(a) (see movie 3 of Supplemental material [12]). The data were computed by taking the average of distributions of speeds in each time frame. This curve shows that in the collective phase the typical swimming speeds range from $20 - 150$ μm/s, with a peak at ~ 60 μm/s, so the collective speeds are significantly larger than the typical individual free swimming speeds. This observation also agrees with previous results [10, 11, 39]. It has been previously suggested [10, 11] that this is a hydrodynamical effect associated with drag reduction and mutual advection equivalent to phenomena observed in sedimentation processes [47].

Obtained in the same way, a speed distribution in a semidilute suspension exhibiting no apparent organized behavior (or subcritical) is shown in blue. The striking feature of this distribution is that the typical speeds are considerably lower than those for free swimming cells. We propose in Sec. IV that this decline occurs when cell to cell separations are sufficiently small to produce a high probability of collisions, but not small enough to trigger collective organization by steric and/or hydrodynamic interactions.

In order to analyze the orientational dynamics in the ZBN mode, we utilize an order parameter introduced elsewhere [11] which measures the level of coherent directional motion in the velocity field. This scalar field Φ_R is defined by the local average $\langle \cos\theta \rangle_R$ of the scalar product of adjacent unit velocity vectors over a small region defined by R,

$$\Phi_R(i,j,t) = \frac{1}{N_R} \sum_{(l,m)\in B_R(i,j)} \frac{\mathbf{v}_{ij}(t) \cdot \mathbf{v}_{lm}(t)}{|\mathbf{v}_{ij}(t)||\mathbf{v}_{lm}(t)|}, \tag{2}$$

where $\mathbf{v}_{ij}(t)$ is the measured velocity field and $B_R(i,j)$ is a quasi-circular region of radius R, centered at (i,j), containing N_R elements. Φ_R can be used to picture the local levels of organization in the system. When $\Phi_R \sim 1$ the vectors inside B_R are nearly parallel, corresponding to phalanxes of coherent motion. Values close to zero indicate strong misalignment, and hence random, disorganized, orientations in R. Negative values imply locally opposing streamlines. Notice that the only information used is the relative direction of motion of the cells in the small region, the modulus of their speeds is not considered. The resolution and level of detail in this analysis are determined by the choice of R. Features in the orientation field smaller than the scale defined by R can not be resolved. An example of an instantaneous contour map of Φ_R is shown in Figure 4(a), with the value $R = 18.91$ μm, corresponding to 6 grid units in the PIV analysis. Since the PIV data is smoothed with a 3×3 spatial filter, this value of R is appropriate to measure the local continuity without undesirable loss of detail.

Using the information given by Φ_R, we can filter velocity vectors from regions with particular levels of organization. For instance, the distribution of magnitudes of the vectors contained in regions in which $0.98 < \Phi_R < 1$, corresponding to a relative angular dispersion of $\lesssim 10^\circ$, is shown in green in Fig. 3. These correspond to very organized regions shown in the darkest tone of red in Fig. 4(a). In the same way, a PDF of vectors within regions with $-0.15 < \Phi_R < 0.15$, i.e. non-coherent motion with average angular dispersion in the range $[80^\circ, 100^\circ]$, is shown in orange in Figure 3(b). The two distinct levels of organization clearly produce radically different distributions of velocity vectors, indicating that the high levels of coherence correspond to fast moving regions, while the regions presenting random orientations correspond to slow motions. A simple conclusion from this observation is that cells located at the boundary between coherent regions are in a jammed mode. This implies that in the ZBN phase cells inside of disordered regions are less concentrated and rapidly colliding and reorienting, like in the subcritical phase, possibly trapped between large moving phalanxes, in a process equivalent to a traffic jam. Eventually these cells get recruited into nearby coherent jets and their motion is reactivated with the addition of the possibility of very close intercellular distances .

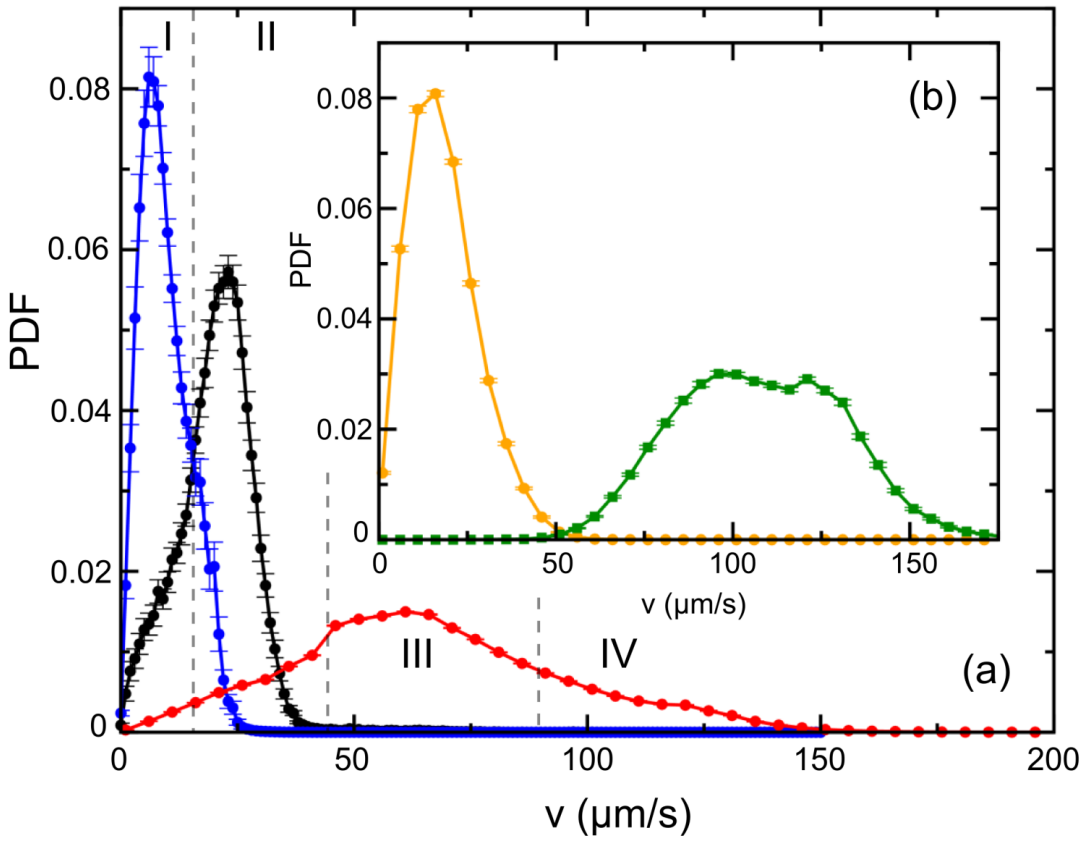

FIG. 3: (Color) Probability distribution functions of speeds. (a) (Black) free swimmers in dilute conditions ($n = (9.7 \pm 1.1)$x10^7 cells/cm^3); (blue) subcritical, or semi-dilute, suspension ($n = (3.39 \pm 0.32)$x10^9 cells/cm^3); (red) ZBN suspension ($n = (4.92 \pm 0.46)$x10^9 cells/cm^3). (b) For the same data shown in red, distribution functions filtered according to order parameter Φ; (green) highly organized regions within the ZBN phase ($0.98 < \Phi < 1$); (orange) isotropic regions within ZBN ($-0.15 < \Phi < 0.15$). Regions I-IV are coarse divisions of the velocity range.

These results are supported by the high spatial correlation between organization level and motion. A contour map with four levels of speeds (termed zones I-IV) as given in Figure 3(b), is shown in Fig. 4(b). White represent slow regions (I), light gray indicates the regions with the free swimming regime (II), dark gray indicates typical collective speeds (III) and black shows very fast regions (IV). Comparison of Figs. 4(a) and 4(b) clearly reveals not only that the global distributions show larger typical speeds for the ZBN phase relative to dilute suspension, but also, at the local level, regions of high directional coherence are directly related to regions of faster motion and *vice versa*. Furthermore, very fast cells, moving in excess of 90 μm/s, are located in the center of large coherent regions. Figure 4(c) is a plot in the space of speed and (positive) Φ_R for all frames analyzed, where color coding indicates local frequency of events for a given combination of speed and Φ_R. The clear accumulation of points confirms that fast cells are always highly organized, and very slow cells are likely not very organized. This is clear proof that speed and co-directional motion in the vicinity of each cell are highly correlated.

IV. DISCUSSION OF VELOCITIES IN THE DISORDERED PHASE

To understand how short cellular mean free paths may lead to anomalously low swimming speeds we consider the details of bacterial propulsion. *B. subtilis* swim by rotating their numerous helical flagella, which are attached to their cell body by flexible joints [48]. Locomotion is accomplished when these filaments wrap around each other to form a flagellar bundle oriented opposite to the direction of motion. This bundle of rotating stiff helical filaments constitutes a low Reynolds number propeller [49–51]. When swimming bacteria collide with each other or with an inert object [52], the bundle of flagella may disperse, and then re-form. The bacteria then continue swimming at some arbitrary angle with respect to its original trajectory. If, for instance, the bundle re-forms at 180° to its former direction,

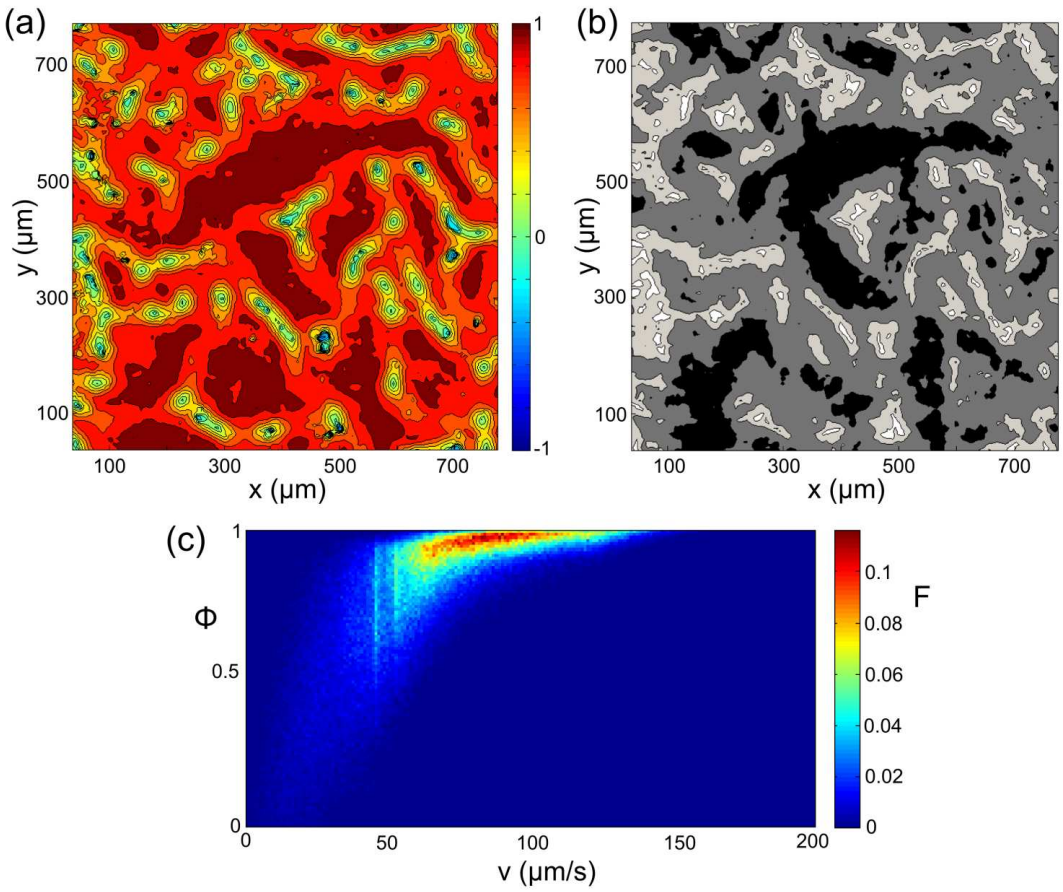

FIG. 4: (Color) (a) View of the contour levels for the orientation field Φ_R in a snapshot of a ZBN sample ($R = 18.91$ μm). (b) for the same frame as in (a), contour levels for values of speeds located in four intervals defined in Fig. 3: white - region I, with speeds < 15 μm/s, light gray - regions II, speeds in the interval 15 μm/s$< v <$ 45 μm/s, dark gray - regions III, with speeds in the interval 45 μm/s$< v <$ 90 μm/s, and black - region IV, with speeds > 90 μm/s. Taking Figure 3 into consideration, these intervals correspond to regions characterized by: jamming (white), free motion (light gray), typical collective motion (dark gray) and super fast motion (black). (c) contour levels of the density of events F for each point of the plane $V - \Phi$, showing the relation between coherent motion and large speeds. Coherent regions are fast and slow regions tend to be disorganized, as evident from comparing (a) and (b).

the organism swims in approximately the direction opposite to the original, leaving the orientation of the cell body unchanged. These polarity reversing flipping events can convert steric co-alignment into unipolar alignment. In the context of subcritical collisions discussed here, cell reorientations reduce the mean speed of the population. It has not been possible to observe this process in concentrated suspensions, as it has at low concentrations [52]. From these experimental results [52] we infer the time needed to resume normal swimming speed is about one second. Thus, if strong collisions occur every fraction of a second, causing frequent dispersal and reconstitution of the flagellar bundle, the mean swimming speed would be less than found along unhindered trajectories. The re-orientation and re-bundling of the flagella yields a model of accelerated motion between collisions. By way of comparison, note that the existence of a finite time for cellular reversals has been suggested to play a role in pattern formation exhibited by myxobacteria [53].

Data on reversals of bacterial locomotion at obstacles [52], shown in Fig. 5a, indicate that the transition from stopped to free swimming is (empirically) described by a time-dependent speed

$$v(t) = v_0 \left(1 - \mathrm{e}^{-t/\tau}\right) \ , \tag{3}$$

with $v_0 \sim 25\mu$m/s the free-swimming speed and $\tau \sim 0.35$ s the acceleration time. Since the orientation of cell trajectories in semi-dilute conditions is still uniformly random, the scattering cross section is close to that of lateral collisions. It is therefore likely that cells stop and restart during many of the interactions in subcritical suspensions.

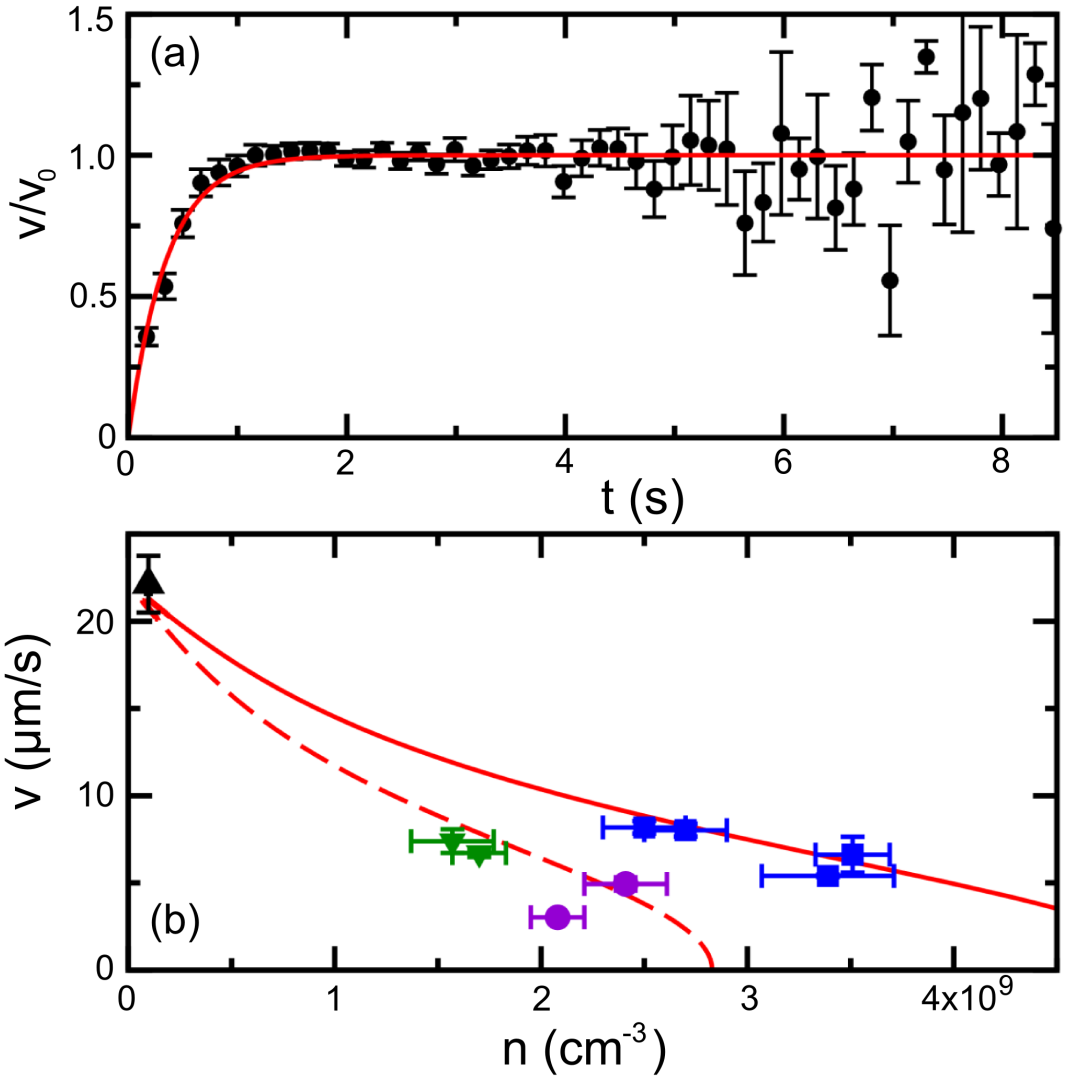

FIG. 5: (Color) Flagella bundling kinetics and its implications. (a) Time dependence of swimming speed after a stop followed by a reversal of swimming direction due to flipping of the flagellar bundle, not by turning of the cell body. Data (solid black circles) from particle tracking velocimetry on many individual cells, shown over a greater time range than originally presented [52]. The data is fitted to Eq. 3 (red), where v_0 is the terminal velocity of each tracked cell. The characteristic time is $\tau = 0.35$ s. The cell acceleration from rest is related to the formation of the flagellar bundle. (b) Expected speeds (Eq. 10) as a function of cell concentration n in subcritical conditions for two excluded volume geometries, $L = 10\mu$m and $D = 2.5\mu$m (solid red line) and $L = 18\mu$m and $D = 2.5\mu$m (dashed red line), as defined in Fig. 6. Data points (solid blue squares, magenta circles, green downward triangles) from several experiments are presented as well. The black upward triangle in the upper left corner indicates the dilute case.

The empirical function (3) implies

$$\frac{x}{v_0\tau} = -\frac{v}{v_0} - \ln\left(1 - \frac{v}{v_0}\right) \ , \tag{4}$$

which gives the length x necessary for a cell to accelerate to a velocity v. We now require an estimate of the free swimming time between collisions, or the mean free path, as a function of the cell concentration. We employ well-established geometrical arguments [54].

We model cells as rigid cylindrical rods of length L and diameter D, with a uniform concentration n and an orientational distribution $\Psi(\hat{\mathbf{k}})$, where $\hat{\mathbf{k}}$ is a unit vector along the long axis of the rod. Consider now an evaluation cylinder Π, with diameter D and length ℓ along the axis of a test particle with length L and orientation $\hat{\mathbf{k}}$, as is shown

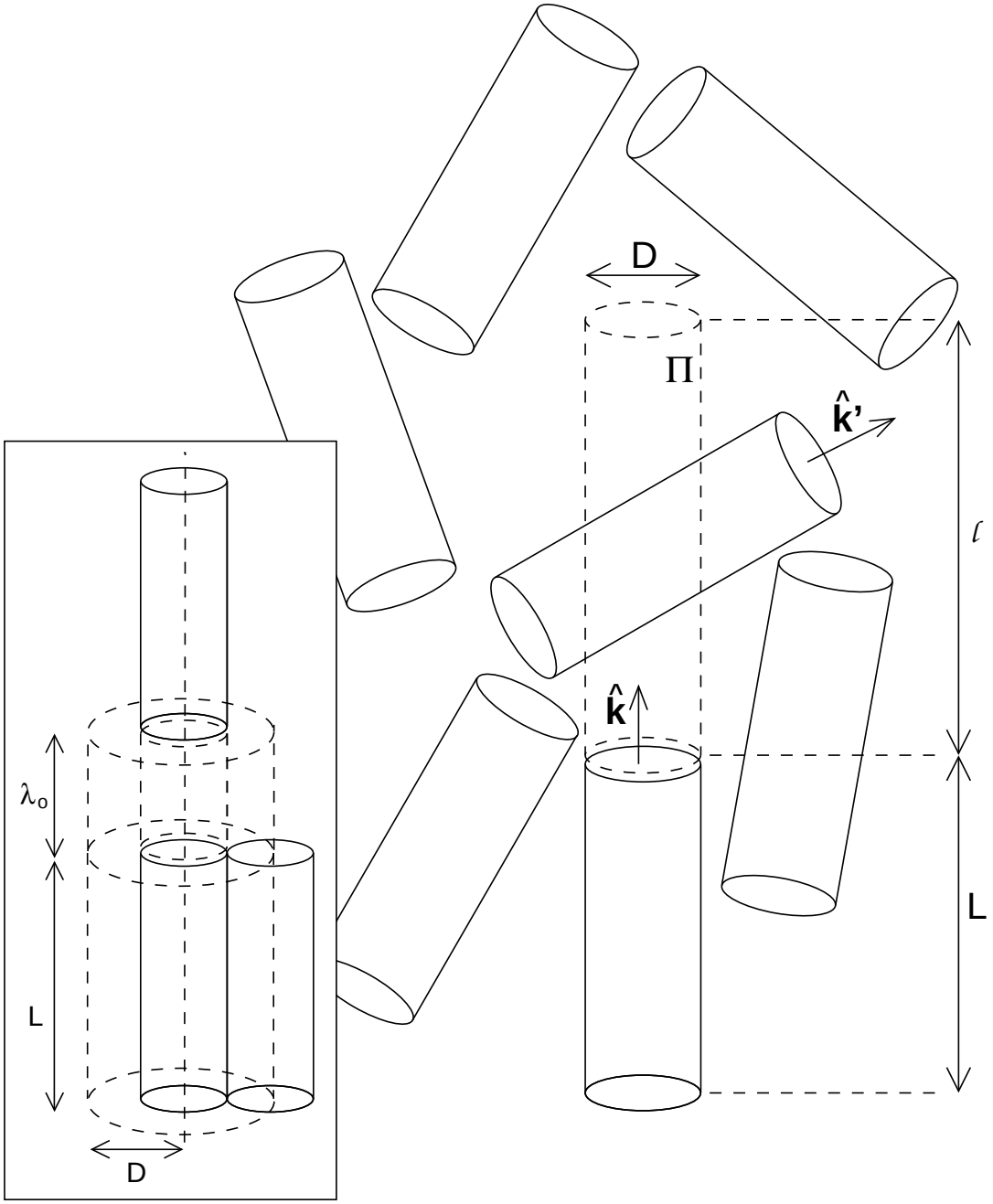

FIG. 6: Geometry of excluded volume. In a suspension of rods of length L and diameter D with a concentration n assumed homogeneous. Consider an evaluation cylinder Π of length ℓ and diameter D located at one end and parallel to a test rod with orientation $\hat{\mathbf{k}}$, the number of rods with orientation $\hat{\mathbf{k}}$ intersecting Π can be accounted as $N = nV_E(\hat{\mathbf{k}}', D, \ell, \hat{\mathbf{k}}', D, L)$ given by Onsager's excluded volume [55]. In the inset: for a polarized configuration, a excluded cylinder with radius D contains one single cell when its length is $1/(n\pi D^2) = L + \lambda_o$; where λ_o is the distance between rods.

in Fig. 6. Rods with orientation $\hat{\mathbf{k}}'$ intersecting Π are those whose center of mass are located in the excluded volume given by Onsager's classic solution for cylinders with spherical caps [55, 56]:

$$V_E(\hat{\mathbf{k}}, \ell, \hat{\mathbf{k}}', L) = \frac{4\pi}{3}D^3 + \pi D^2(\ell + L) + 2DL\ell|\hat{\mathbf{k}} \times \hat{\mathbf{k}}'| \ . \tag{5}$$

For aspect ratios $L/D \gtrsim 4 - 5$ the first term can be neglected, and the average number of rods intersecting Π can be

written as

$$N = \left\langle nV_E(\hat{\mathbf{k}}, \ell, \hat{\mathbf{k}}', L) \right\rangle_{\hat{\mathbf{k}}'} \simeq \pi n D^2(\ell + L) + \frac{\pi}{2} n D L \ell G(\hat{\mathbf{k}}) \ , \tag{6}$$

with

$$G(\hat{\mathbf{k}}) = \frac{4}{\pi} \left\langle |\hat{\mathbf{k}} \times \hat{\mathbf{k}}'| \right\rangle_{\hat{\mathbf{k}}} = \frac{4}{\pi} \int d\hat{\mathbf{k}}' \Psi(\hat{\mathbf{k}}') |\hat{\mathbf{k}} \times \hat{\mathbf{k}}'| \ . \tag{7}$$

An isotropic distribution has $\Psi_I = 1/4\pi$ and $G_I = 1$, while in a polarized system $\Psi_P = \delta(\hat{\mathbf{k}}' - \hat{\mathbf{k}})$ and $G_P = 0$.

The typical distance that a cell is free to translate along its axis before hitting another cell can be obtained by considering $\ell = \lambda(n)$ such that $N \sim 1$. This gives the definition of the mean free path:

$$\lambda(n) = \frac{\lambda_o}{1 + \frac{1}{2} s G(\hat{\mathbf{k}})} \ , \tag{8}$$

where $s = (L/D)$ is the aspect ratio and $\lambda_o = (n\pi D^2)^{-1} - L$. When the system is polarized the mean free path is exactly the expected spacing between aligned rods, $\lambda_P = \lambda_o$ (see inset in Fig. 6). On the other hand, for an isotropic distribution $\lambda_I = \lambda_o(2/(s+2)) < \lambda_o$. To summarize, the typical mean free path increases with the level of alignment, measured by $G(\hat{\mathbf{k}})$, and is inversely proportional to n (or to the volume fraction $\phi = nV_i$ with $V_i = \frac{\pi}{4} D^2 L$ the volume of a single rod).

Now, for a particular value of the concentration n, the condition $x = \lambda(n)$ restricts the maximum velocity achievable by a cell, as given by (4). But of course in a given experiment cells do not stop and resume motion in a synchronized way. Assuming the system is ergodic, an estimate of the most likely velocity observed is

$$< v >= \frac{1}{T} \int_0^T v(t) dt \ , \tag{9}$$

with T the mean free time such that $x(T) = \lambda(n)$ (*i.e.* $T = T(n)$). This gives

$$< v > = v_0 - \frac{\tau}{T} v(T) = \frac{\lambda(n)}{T(n)} = \frac{2}{(s+2)T(n)} \left(\frac{1}{n\pi D^2} - L \right) \ . \tag{10}$$

Figure 5(b) shows experimental results for $< v >$ versus n for different subcritical samples along with corresponding theoretical curves using two assumptions for the size parameters (with $D = 2.5\mu$m): solid red is for $L = 10\mu$m and dashed red is for $L = 18\mu$m). All data points shown as solid squares were produced using the same initial bacterial culture, while the others (solid circles, downward triangles) arise from two different cultures. The parameter L is the length of the flagellar envelope around single cells. It is known that under different growth conditions bacteria can develop flagella of different lengths. This type of biological control was not implemented in our experiments. It is plausible that these data points correspond to cells of different effective lengths. The data shown in solid blue matches our theoretical description remarkably well.

Steric repulsion between cells should be considered for concentrations $n \geq n_E = 1/\tilde{V}_E$, where

$$\tilde{V}_E = \left\langle V_E(\hat{\mathbf{k}}, L, \hat{\mathbf{k}}', L) \right\rangle_{\hat{\mathbf{k}}'} \sim \frac{\pi}{2} D L^2 + 2\pi D^2 L \tag{11}$$

is the average excluded volume of a rod in an isotropic distribution [55, 56]. The corresponding volume fraction is $\phi_E = 1/(2s + 8)$. We deem this to be a lower bound on the semidilute concentration regime, where the rods can no longer be considered totally independent. For the case of *Bacillus subtilis*, if only the cell body is taken into account ($L \sim 4\mu$m and $D \sim 1\mu$m) then $n_E \sim 2 \cdot 10^{10}$ cm^{-3} ($\phi_E \sim 0.062$). But a more realistic analysis must include the effect of the flagella around each organism. In this sense, even though the flagellar envelope is not a rigid structure, its volume exclusion can be accounted for simply by considering a larger size rod. For instance, with $L \sim 10$ μm and $D \sim 2.5$ μm, for which the aspect ratio s is conserved, $n_E \sim 1.3 \cdot 10^9$ cm^{-3} . Under isotropic conditions, the mean free path at this concentration is given $\lambda_{I,E} = L$. At $n \sim n_E$ cells typically occupy the excluded volume of one other cell. In particular, the average number of contacts that a cell has is $N_c = nV_E = n/n_E$ [57, 58]. This is a convenient normalized concentration, which clearly indicates the proximity of the cells in terms of interactions. For

concentrations close to n_E the number of contacts per cell is few. Even though this is an evident constraint on the orientations of cells, at this level there is still a wide range of orientation configurations available for each of them. Cells are somewhat restricted to translate along their axis but otherwise free to take almost any orientation. For concentrations as high as $5n_E$, a system of inactive rods reaches a typical random packing condition [59]; for $\sim 10n_E$ they display a transition into liquid crystalline phase [55, 56, 58].

We conclude that $\lambda < L$ for isotropic symmetry and concentrations $n \gtrsim n_E$, and hence the typical cell speeds can be much smaller than the free swimming values. That is, for semi-dilute conditions, cells cannot reach their terminal velocity before a collision occurs, yielding a permanent state of re-orientation. This condition also implies that the uniform random distribution of cell orientations is stationary. As more cells are packed together, steric repulsions starts to induce local alignment, in the manner of a liquid crystal, as predicted by Onsager's theory. The reorientation of the cells will then be highly restricted, inducing local co-alignments and a consequent increase of the mean free path λ.

The above analysis assumes implicitly that the test cell is the only one moving, and it neglects hydrodynamic interactions. Clearly the flows induced in the surrounding fluid by an active particle produce changes in the trajectories of other particles in the vicinity [60–64]. These interactions are at least partially responsible for the collective phenomena emerging in these systems. In the case of flagellated bacteria, like *B. subtilis*, such interaction tend to align them, inducing a bias in $\Psi(\mathbf{k})$. Therefore the assumption that the distribution of cells stays isotropic is not correct in principle, as cell-cell interactions induce local alignment. But for a semi-dilute system, this process is not necessarily stable, as the cells can reorient randomly after each frontal collision loosing spatial correlation. Due to frequent collisions, the system can quickly regain the isotropic distribution. Also under these circumstances cells can not reach very fast speeds, so the hydrodynamic interactions are weakened. In this way the assumption of stationary isotropic state for a semi-dilute system is justifiable. Equation 8 gives an estimated lower bound on the mean free path for subcritical concentrations. For larger concentrations this assumption breaks down due to significant steric repulsions associated to the volume exclusion, which now restricts not only translations but also rotations of the cells, breaking the isotropic symmetry into the organized behavior. In this case it is necessary to introduce a Fokker-Planck equation to describe the correlation between cell orientations, motion and concentration fields [19–21]. In particular, if all the cells are moving in the same direction with the same speed, only very few collisions are expected, as they just follow each other in line. For a less ideal case, the collision distance will depend on the distribution of speeds as well as the distribution of orientations. The point to be made is that the mean free path is short for an isotropic system and long for an organized one. The parameter λ_o is determined by the typical distance between cells, given by the number concentration n. The fact that the isotropic mean free path is λ_o/s indicates that the restriction on the length scale is purely a geometrical fact: for slender rods λ_I will be very short. Steric alignment determines a reduction in the value of the geometrical factor G, inducing an increase of the mean free path, while at the same time yielding a situation in which cells are moving close to each other, inducing large flows due to directed collective propulsion.

A final point to be made in this regard concerns recent theoretical studies [65, 66] of the development of orientational order in systems of 'self-propelled rods' which interact by a soft-core volume exclusion and without any long-range hydrodynamic interactions. Numerical studies by Peruani, Deutsch, and Bär [65] show the emergence of clusters with a broad distribution of sizes at a critical volume fraction that depends sensitively on the aspect ratio of the particles. This onset point can be considerably less than the equivalent non-moving system's ordering transition as described by the Onsager criterion. But bearing in mind that such simulations do not take into account partial stopping and acceleration of cells during and after their interactions due to breakdown of the propelling flagella bundle, clearly relevant in real bacterial systems, we can expect that such a work gives a lower bound to the critical cell concentration. The dynamics of the cluster size distribution function involves consideration of the scattering cross section of the rods analogous to that which we have employed above. The order found in these works is intrinsically polar, like that seen here. Similar results we obtained by Yang, Marceau, and Gompper [66] who studied the more general problem in which the particles could undulate like flagella and thereby synchronize their motion. In addition to the appearance of ordered, polar clusters it was also found possible to develop a jammed system, reminiscent of the intermediate phase discussed here.

V. CONCLUSIONS

The experiments and analysis reported here have shown that suspensions of at least one species of rod-shaped self-propelled bacteria exhibits a succession of phases as the concentration of these organisms increases from dilute to close packed. Individual swimming speeds of free cells obey a bell-shaped distribution peaked at ~ 25 μm/s. At higher intermediate concentrations the speed distribution is collision-dominated while cell body orientations are still isotropically distributed. This stage corresponds to a "jammed" phase with a distribution peaking at much lower

speeds than the distribution for individuals. The jammed state can be explained by the combination of frequent collisions, reorientations and deployment-reconstitutions of the flagellar bundle. Speeds in the high concentration phase peak at considerably higher values than those of individual cells. These speeds characterize the motion of aligned, nearly close packed bacteria swimming co-directionally, equivalent to a dense highway traffic. Enhanced speeds in this mode are highly correlated to the degree of co-alignment and proximity of the swimmers. It has been shown [11] that the anomalously rapid propulsion of a phalanx, during an interval of coherence, can be due to propulsion by bacteria located at and near its boundary. Recent work [67] measuring directly the flow fields around freely-swimming bacteria shows that hydrodynamic interactions between cells are washed out by rotational diffusion beyond a few microns, so it is only when the intercell-spacing is smaller would the enhanced speeds appear. We have shown that the ZBN phase is locally characterized by directional order correlated with high collective velocities of an ordered domain. These domains are "phalanxes" since the members of them are tightly adjacent and move co-directionally. What could be their origin? We speculate, but have no direct evidence, that the ZBN phase is actually a pair of successively developing phases, the first a steric alignment of rods, as described by Onsager [55], followed by a flip of bundles [52] of the propelling flagella of the rods, a.k.a. bacteria, that are not swimming in the direction of the local majority, so as to give a unidirectional, i.e. polar, collective alignment. The origin of intermittency, the instability of the phalanxes, resulting in the appearance of "turbulence," is currently under investigation. It should be noted that at the high concentrations of the ZBN it is difficult to determine the local variations in cell concentration, but these would be expected to be correlated with the speed and local orientation as well, and current research aims to study this effect. Due to intermittency, phalanxes travel for a short distance, followed by break-up and reconstitution in new directions. The ZBN is therefore an efficient mixing phase. Quantitative analysis of this mixing is an important future goal. Since bacteria require a continual supply of metabolites, e.g. oxygen, and a dispersal of waste exudates, this dynamic property of the ZBN is of considerable significance in the life and environmental interaction of these bacteria.

Is there evidence for universality? The occurrence of a ZBN phase is not restricted to wild-type *B. subtilis* cells. We have shown that "run only" *B. subtilis* (a gift of George Ordal) also exhibit a ZBN phase. From this we infer that intermittency in the formation and breakup of coherent phalanxes of these swimming bacteria is not due to run-and-tumble transitions [33].

Do species other than *B. subtilis* undergo the ZBN phase transition? *Erwinia carotivora*, gram negative rod-shaped soil-dwelling bacterial cells, also exhibit a ZBN phase (J.O. Kessler, M. Hawes, G. Curlango, unpublished). The minimum inference to be drawn is that occurrence of the ZBN phase is not restricted to one species of bacteria. Tests are planned to determine whether only rod-shaped peritrichously flagellated cells exhibit the phenomenon. It seems likely, however, that parallel alignment of swimmers requires the packing characteristics of concentrated rods.

Is the phenomenon limited to laboratory experiments? Concentrated populations of aerobic bacteria can occur when the aqueous medium that suspends them is rich in nutrients and oxygen. If the bacterial suspension has a slanted interface, as in sessile drop cultures [10] or on wetted grains of soil or sand (the natural habitat of *B. subtilis*) the organisms concentrate themselves, with the aid of gravity. Such circumstances require enhanced transport and mixing, e.g. of oxygen from the surface of the suspension and of CO_2 out of it. Mixing and transport from the boundaries of a ZBN culture, and within it, are major consequences of the dynamics and intermittency. Thus, while the occurrence of the ZBN phase might be "an accident," it is an accident whose occurrence is welcomed in producing enhanced viability.

We believe that the insights into the occurrence and character of the ZBN phase, presented in this paper, open new avenues of research for the physics of active matter, and furthermore suggest new insights into microbial dynamics within aqueous environments.

Appendix: Calibration of the PIV method

The cross-correlation of two scalar fields I_1 and I_2 as a function of the shift (x, y) is defined as

$$C_\Gamma(x,y) = \frac{\iint_\Gamma I_1(x',y') I_2(x'+x, y'+y) dx' dy'}{\iint_\Gamma I_1(x',y') I_2(x',y') dx' dy'} \ , \tag{A.1}$$

where Γ is the subspace in which the correlation is evaluated. Considering digital images, I corresponds to bit level values per pixel (e.g., for 8-bit gray scale images, integers $[0, 255]$). In this case, C_Γ can be written in terms of summations over discrete coordinates $(x', y') = (x'_i, y'_i)$.

The PIV method consists of finding the shift (x^*, y^*) which gives the maximum value of C_Γ. This can be done by evaluating C_Γ for all possible values (x_i, y_i), generating a discrete correlation landscape and using the maximization method of choice. For two sequential images I_1 at time t and I_2 at time $t + \Delta t$, with Δt the time increment between

frames, (x^*, y^*) is the most likely displacement of the features imaged in the evaluation window Γ. In this way, the average velocity of the particles contained in Γ is simply given by

$$(u, v) = \frac{1}{\Delta t}(x^*, y^*) \tag{A.2}$$

This procedure is repeated for all possible evaluation windows Γ in each frame, to generate a two dimensional vector field of velocities. To decrease the computational cost of this process, most applications use Fourier methods to reduce the implicit summations in the cross correlation function into multiplications of complex coefficients.

Extensive introductions to PIV methods can be found in the literature [41, 43, 68, 69]. Many different correlation algorithms and other related procedures have been proposed, carrying out sophisticated methods of analysis, including the implementation of predictors based on previous history, adaptive window sizing and off-setting, window deformation and vector validation methods [70], continuous window shifting [71], histogram equalization methods [72], and others.

The determination of the displacement (x^*, y^*) can be achieved with sub-pixel accuracy by use of a linear regression fit of $C_\Gamma(x, y)$ around the peak value in the discrete landscape. If the typical displacements are small relative to the pixel size then sub-pixel precision is clearly crucial. But an inherent systematic error is unavoidable when using the conventional procedures: an integer bias caused by an asymmetry inherent from the discrete sampling of the correlation landscape around it. This issue is called the Pixel Locking Effect [43, 69, 71, 73–77], and although it can be minimized, its emergence is independent of the correlation algorithm used. Unfortunately, due to the combination of length and time scales of ZBN, this error is of particular significance for the analyses presented in this paper. For instance, in our experimental conditions we expect the cell velocity probability distribution to be invariant under rotations, because the boundaries of the system are far away and there is no intrinsic mechanism to break such a symmetry. Yet, if we examine the distribution of velocities as reported by the PIV software, we observe that it has

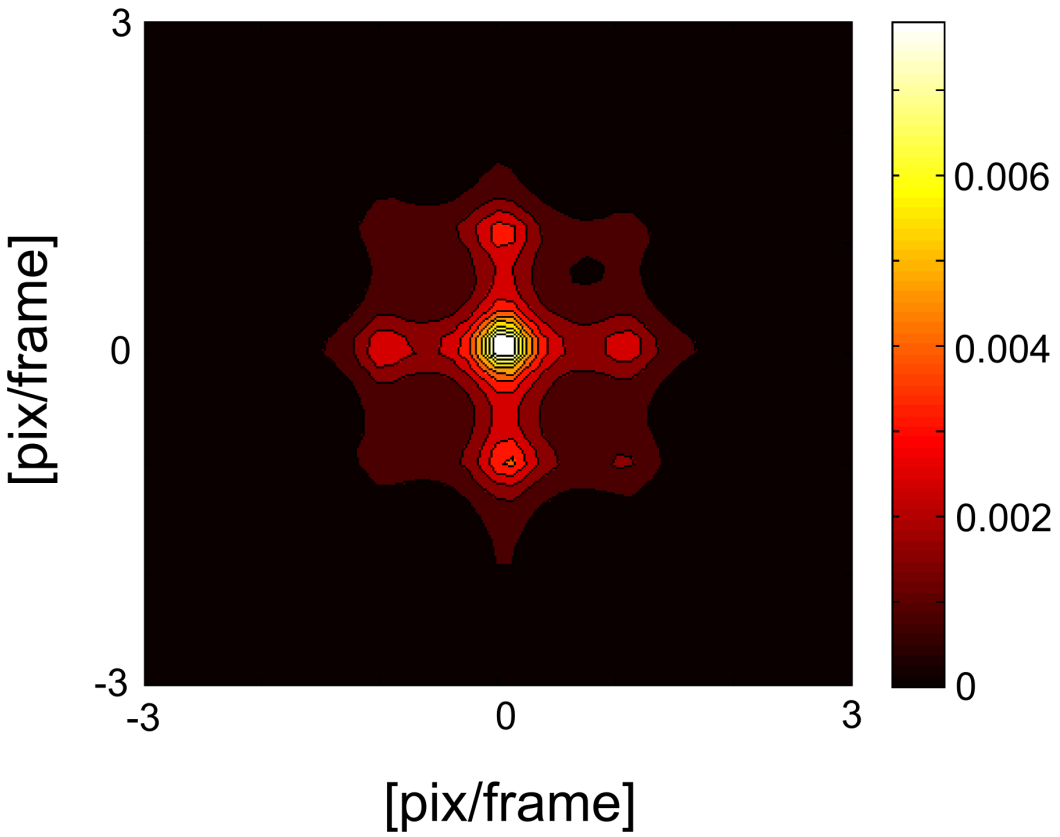

FIG. 7: (Color) Two dimensional distribution of displacements in a sample of swimming bacteria. Axes indicate displacement components in pixels from a frame to the next one, as reported by PIV, while the color indicates the frequency of occurrences (see colorbar). The system is inherently isotropic, and this distribution function should be symmetric with respect to rotation around the origin in the XY plane, which is clearly not the case.

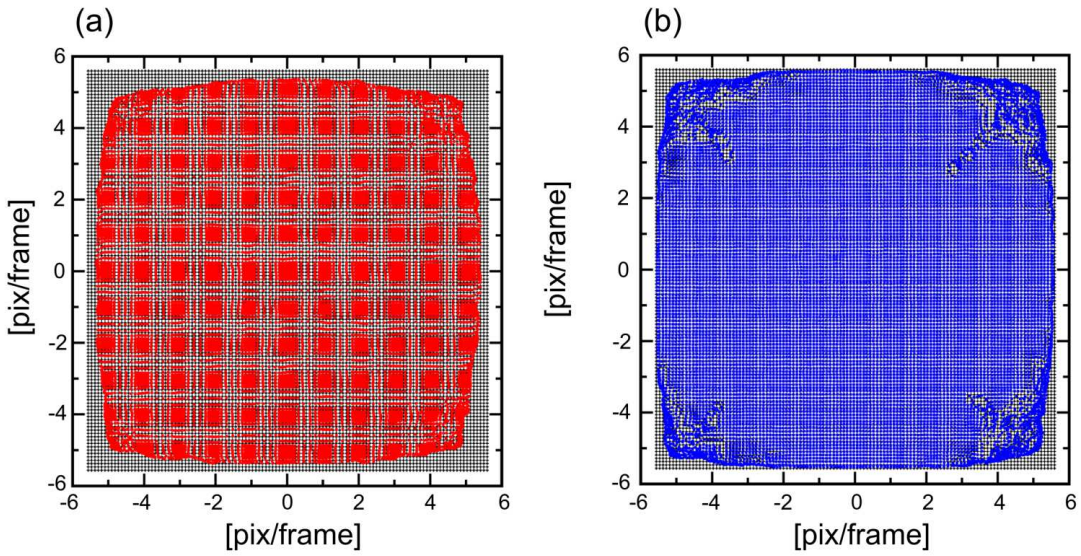

FIG. 8: (Color) Details of pixel-locking analysis. (a) Test case phase space: black dots indicate real values of (U, V), red points indicate corresponding (u, v) measured by PIV. As is evident, velocities are underestimated in a particular pattern, as shown in Figure 9. (b) Real phase space (U, V) (black) and corrected phase space (U', V') (blue).

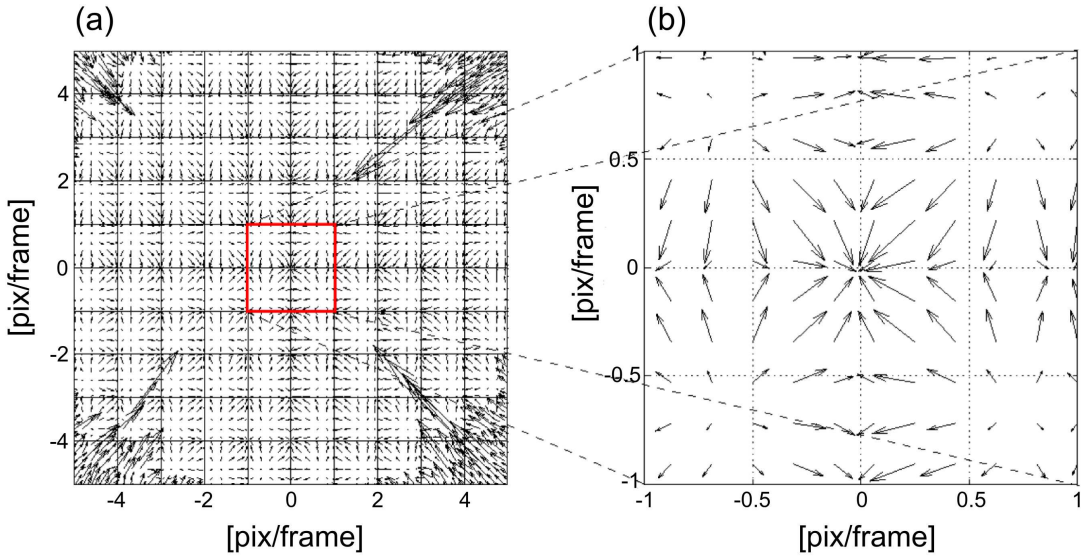

FIG. 9: (Color) Residuals. This vector map shows the difference (R_u, R_v), indicating how each of the points of the test images space are mapped into the PIV space. This shows how the points in the velocity space are moved towards integer values, and away from fractional integer values.

an obvious lattice bias (Fig. 7), a hallmark of a systematic pixel locking error.

Some previous work had been done with regard to correcting this issue: in [73] the asymmetry around the integer peak was compensated by a constant factor before using a symmetrical Gaussian function; in [72] a histogram equalization method is used to adjust speed distributions, but no correction to the vectors is done; in [71] a continuous window-shifting method is implemented; [78] claims to solve the systematic error problem using the correlation mapping method, which consist of combining interpolation of images and window shifting to evaluate the correlation function and in [77] sine functions are used to fit the residual error and correct it.

We introduce here a technique to characterize the error and produce a simple calibration process. The intention is to use this method with a commercial PIV system without modifying the PIV process itself. In other words, our

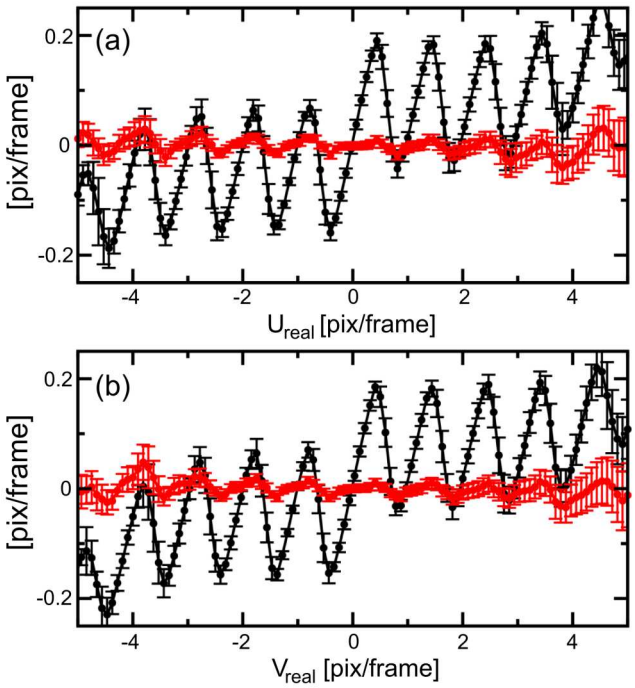

FIG. 10: (Color) Residuals of uncorrected data $R_U = U - u$ (a) and $R_V = V - v$ (b) are shown in black and corrected data $R'_U = U - U'$ (a) and $R'_V = V - V'$ is shown in red. In both cases the pixel locking phenomenon is obvious if the field is not corrected. Error bars represent dispersion of the data for each location, and should be a good estimate of the confidence of the measurement. These dispersions are related to random errors such as particular seedings within a single evaluation window for different time frames.

effort is oriented to reduce the systematic pixel locking effect by adjusting data as a post-processing procedure. To calibrate the PIV system, a known field must be measured with it, and the obvious way to implement this is to produce a digital movie of simulated particles moving according to a prescribed field. In order to have the same seeding conditions as those of the real system in question, we take a snap shot of it (see Fig. 1) and perform image rotations using the standard bi-cubic extrapolation method . Therefore the "real" field is well known. The simulated dynamics is henceforth analyzed with PIV using the same parameters and settings as for the experimental data (see section II). Two hundred frames are time averaged to produce a single, noise reduced, velocity field. A comparison of the real and the measured field phase spaces is shown in Figure 8a. In this representation, points (U, V) of the prescribed field correspond to a regularly spaced grid of points in the plane (black points in Fig.8a). The phase space of the PIV results, (u, v), is shown as red dots. As is evident, the PIV analysis produces a very peculiar deformation of the field characterized by a systematic bias of the displacements towards integer pixel values, as is nicely portrayed in Figure 9, where the arrows depict the residual vectors $(R_u, R_v) = (u - U, v - V)$.

In order to obtain a usable instrument calibration we need to correct for the pixel locking effect. In principle, a simple inversion of the map shown in Figure 9 should be enough to accomplish this. In this way, if we calculate

$$(U', V') = (u, v) - (R_u, R_v) \tag{A.3}$$

and if the map is robust, we should obtain the corrected field $(U', V') \simeq (U, V)$ The map is constructed using a linear interpolation method. We interpolate the residual field (R_u, R_v) on a square mesh to produce a value look up table (LUT) that can be used to estimate the inverted map. Henceforth, we seek the three closest points, $(u_i, v_i)_{i=1,2,3}$, to each point obtained from PIV analysis, (u, v). Given that we know how those three points are mapped back into the real space (U, V), the corrected velocity value (U', V') can be interpolated from them. Considering the landscapes generated by the LUT points for each component of the real space, $U(u_i, v_i)$ and $V(u_i, v_i)$, the corrected value (U', V') of an arbitrary PIV point (u, v) can be calculated simply by evaluating it in the plane generated by $(u_i, v_i)_{i=1,2,3}$.

In Figure 8b we see the average corrected phase space in blue. Is clear that the inversion almost completely corrects the data, except in the corners of the velocity plane where fluctuations are strong due to scarce large speed readouts. Nonetheless, the corrected field has an almost perfect coverage of the phase space.

Results are shown in Figure 10 in the form of residuals $(R_U, R_V) = (U, V) - (u - v)$ and $(R'_U, R'_V = (U, V) - (U', V')$.

Error bars indicate dispersions around the time average. The wavy shape in the plots has a wavelength of about one pixel/frame, and is related to the square structure shown in Figure 9. This is an evident indicator of Pixel Locking. We see that the corrected data does not entirely eliminate this feature, but decreases its amplitude considerably. The residual wave has an amplitude of about 1/20th of a pixel/frame displacements, providing a confidence level of about ± 0.05 pixels.

This work was supported by the U.S. DOE, Office of Basic Energy Sciences, Division of Materials Science and Engineering, Contract DE AC02-06CH11357, and the European Research Council, Advanced Investigator Grant 247333.

[1] *Bacteria as Multicellular Organisms*, edited by J.A. Shapiro and M. Dworkin, (Oxford University Press, Oxford, UK, 1997).
[2] J.A. Shapiro, Annu. Rev. Microbiology **52**, 81 (1998).
[3] L. Hall-Stoodley, J.W. Costerton, and P. Stoodley, Nature Rev. Microbiol. **2**, 95 (2004).
[4] J. Henrichsen, Bacteriol. Rev. **36**, 478 (1972).
[5] D. Kaiser, Curr. Bio. **17**, R561 (2007).
[6] M.F. Copeland and D.B. Weibel, Soft Matter **5**, 1174 (2009).
[7] J.O. Kessler and M. Wojciechowski, in [1], pp. 417-450.
[8] J.O. Kessler and N.A. Hill, in *Physics of Biological Systems, From Molecules to Species*, H. Flyvbjerg et al. eds, Springer Lecture Notes in Physics 480 (Springer, Berlin, 1997), pp. 323-340.
[9] J.O. Kessler, in *Equadiff 99 (1-7 Aug), International Conference on Differential Equations*, Vol 2, B. Fiedler, et al. eds (World Scientific, city, 2000), pp. 1284-1287.
[10] C. Dombrowski, L. Cisneros, S. Chatkaew, R.E. Goldstein, and J.O. Kessler, Phys. Rev. Lett. **93**, 098103 (2004).
[11] L.H. Cisneros, R. Cortez, C. Dombrowski, R.E. Goldstein and J.O. Kessler, Exp. Fluids **43**, 737 (2007).
[12] See supplementary material at XXX for movies of suspensions at various concentrations.
[13] J. Toner and Y.H. Tu, Phys. Rev. Lett. **75**, 4326 (1995).
[14] T. Vicsek, A. Czirok, E. Ben-Jacob, I. Cohen, and O. Shochet, Phys. Rev. Lett. **75**, 1226 (1995).
[15] G. Grégoire and H. Chaté, Phys. Rev. Lett. **92**, 025702 (2004). See also F. Ginelli, F. Peruani, M. Bar, and H. Chaté, Phys. Rev. Lett. **104**, 184502 (2010).
[16] R.A. Simha and S. Ramaswamy, Phys. Rev. Lett. **89**, 058101 (2002).
[17] J.P. Hernandez-Ortiz, C.G. Stoltz, and M.D. Graham, Phys. Rev. Lett. **95**, 204501 (2005).
[18] D. Saintillan and M.J. Shelley, Phys. Rev. Lett. **99**, 058102 (2007).
[19] D. Saintillan and M.J. Shelley, Phys. Rev. Lett. **100**, 178103 (2008).
[20] D. Saintillan and M.J. Shelley, Phys. Fluids **20**, 123304 (2008).
[21] C. Hohenegger and M.J. Shelley, Phys. Rev. E **81**, 046311 (2010).
[22] A. Baskaran and M. Marchetti, Proc. Natl. Acad. Sci. USA **106**, 15567 (2009).
[23] P.T. Underhill, J.P. Hernandez-Ortiz, and M.D. Graham, Phys. Rev. Lett. **100**, 248101 (2008).
[24] C.W. Wolgemuth, Biophys. J. **95**, 1564 (2008).
[25] X.-L. Wu and A. Libchaber, Phys. Rev. Lett. **84**, 3017 (2000).
[26] K.C. Leptos, J.S. Guasto, J.P. Gollub, A.I. Pesci, and R.E. Goldstein, Phys. Rev. Lett. **103**, 198103 (2009).
[27] I. Rushkin, V. Kantsler, and R.E. Goldstein, Phys. Rev. Lett. **105**, 188101 (2010).
[28] T.J. Pedley and J.O. Kessler, Annu. Rev. Fluid Mech. **24**, 313 (1992).
[29] I.S. Aranson, A. Sokolov, J.O. Kessler, and R.E. Goldstein, Phys. Rev. E **75**, 040901 (2007).
[30] H.P. Zhang, A. Be'er, E.-L. Florin,, and H.L. Swinney, Proc. Natl. Acad. Sci. USA **107**, 13626 (2010).
[31] A. Sokolov, I.S. Aranson, J.O. Kessler, and R.E. Goldstein, Phys. Rev. Lett. **98**, 158102 (2007).
[32] E.M. Purcell, Am. J. Phys. **45**, 3 (1977).
[33] H.C. Berg, *Random Walks in Biology*, 2nd edition (Princeton University Press, Princeton, New Jersey, 1993).
[34] C. Pozrikidis, *Introduction to Theoretical and Computational Fluid Dynamics* (Oxford University Press, Oxford, 1997).
[35] I. Tuval, L. Cisneros, C. Dombrowski, C.W. Wolgemuth, J.O. Kessler, and R.E. Goldstein, Proc. Natl. Acad. Sci. USA **102**, 2277 (2005).
[36] A.J. Hillesdon, T.J. Pedley, and J.O. Kessler, Bull. Math. Bio. **57**, 299 (1995).
[37] A.M. Metcalfe and T.J. Pedley, J. Fluid Mech. **370**, 249 (1998).
[38] NA. Hill and T.J. Pedley, Fluid Dyn. Res. **37**, 1 (2005).
[39] A. Sokolov, R.E. Goldstein, F.I. Feldchtein, and I.S. Aranson, Phys. Rev. E **80**, 031903 (2009).
[40] S. Inoue and K.R. Spring, *Video Microscopy: the Fundamentals*, 2nd edition (Plenum, New York, 1997).
[41] C.E. Willert and M. Gharib, Exp. Fluids **10**, 181 (1991).
[42] R.D. Keane and R.J. Adrian, Appl. Sci. Res. **49**, 191 (1992).
[43] A.K. Prasad, Curr. Sci. **79**, 51 (2000).
[44] N. Darnton and J.D. Jaffe, *Particle/Bacterial Tracking Software*, Rowland Institute at Harvard University (2003).
[45] L.H. Cisneros, "Particle Tracking Velocimetry source code for MatLab," available at `www.physics.arizona.edu/~cisneros/codes/PTV/`.

[46] J.O. Kessler, G.D. Burnett and K.E. Remick in *Nonlinear Science at the dawn of the 21st Century*, P.L. Christensen *et al.* eds, Springer Lecture Notes in Physics 542 (Springer, Berlin 2000), pp. 409 -426.
[47] I.M. Jánosi, T. Tél, D.E. Wolf, and J.A.C. Gallas, Phys. Rev. E **56**, 2858 (1997).
[48] F. Samatey, H. Matsunami, K. Imada, S. Nagashima, T. Shaikh, D. Thomas, J. Chen, D. DeRosier, A. Kitao, and K. Namba, Nature **431**, 1062 (2004).
[49] R. Anderson, in *Swimming and Flying in Nature*, ed. T. Wu, C. Brokaw, and C. Brennan (Plenum, New York, 1975), vol. 1, pp. 45-56.
[50] R. Macnab, Proc. Natl. Acad. Sci. USA **74**, 221 (1977).
[51] J. Lighthill, SIAM Rev. **18**, 161 (1976).
[52] L. Cisneros, C. Dombrowski, R.E. Goldstein, and J.O. Kessler, Phys. Rev. E **73**, 030901(R) (2006).
[53] U. Borner, A. Deutsch, H. Reichenbach, and M. Bar, Phys. Rev. Lett. **89**, 078101 (2002).
[54] M. Doi and S.F. Edwards, *The Theory of Polymer Dynamics* (Oxford University Press, Oxford, 1986).
[55] L. Onsager, Ann. N.Y. Acad. Sci. **51**, 627 (1949).
[56] G. Vroege and H. Lekkerkerker, Rep. Prog. Phys. **55**, 1241 (1992).
[57] A.P. Philipse, Langmuir **12**, 1127 (1996).
[58] A.P. Philipse and A. Verberkmoes, Physica A **235**, 186 (1997).
[59] A. Wouterse, S. Luding, and A. Philipse, Gran. Matter **11**, 169 (2009).
[60] T. Ishikawa, G. Sekiya, Y. Imai, and T. Yamaguchi, Biophys. J. **93**, 2217 (2007).
[61] Q. Liao, G. Subramanian, M.P. DeLisa, D.L. Koch, and M. Wu, Phys. Fluids **19**, 061701 (2007).
[62] C.M. Pooley, G.P. Alexander, and J.M. Yeomans, Phys. Rev. Lett. **99**, 228103 (2007).
[63] E. Lauga and T.R. Powers, Rep. Prog. Phys. **72**, 096601 (2009).
[64] J.P. Hernandez-Ortiz, P.T. Underhill, and M.D. Graham, J. Phys. Cond. Matt. **21**, 204107 (2009).
[65] F. Peruani, A. Deutsch, and M. Bär, Phys. Rev. E **74**, 030904(R) (2006).
[66] Y. Yang, V. Marceau, and G. Gompper, Phys. Rev. E **82**, 031904 (2010).
[67] K. Drescher, J. Dunkel, L.H. Cisneros, S. Ganguly, and R.E. Goldstein, Proc. Natl. Acad. Sci. USA, submitted.
[68] R.J. Adrian, Annu. Rev. Fluid Mech. **23**, 261 (1991).
[69] J. Westerweel, Meas. Sci. Tech. **8**, 1379 (1997).
[70] D.D. A/S *Dantec's software user's guide. flowmanager software and introduction to piv instrumentation* (Skovlunde, Denmark, 2002).
[71] L. Guis and S.T. Wereley, Exp. Fluids **32**, 506 (2002).
[72] G. Roth and J. Katz, Meas. Sci. Tech. **12**, 238 (2001).
[73] H. Huang, D. Dabiri, and M. Gharib, Meas. Sci. Tech. **8**, 1427 (1997).
[74] A.M. Fincham and G.R. Spedding, Exp. Fluids **23**, 449 (1997).
[75] J. Westerweel, Exp. Fluids **29**, 3 (2000).
[76] K.T. Christensen, Exp. Fluids **36**, 484 (2004).
[77] M.R. Cholemari, Exp. Fluids **42**, 913 (2007).
[78] J. Chen and J. Katz, Meas. Sci. Tech. **16**, 1605 (2005).